Study of covalent spin interactions in Cd1-xMnxSe by cryobaric magnetophotoluminescence

Study of covalent spin interactions in $Cd_{1-x}Mn_xSe$ by cryobaric magnetophotoluminescence

N. Kuroda, Y. H. Matsuda,* G. Kido,† and I. Mogi

Institute for Materials Research, Tohoku University, Sendai 980-8577, Japan

J. R. Anderson

Department of Physics, University of Maryland, College Park,

MD 20742-4111, USA

W. Giriat

IVIC, Centro de Fisica, Apartado 21827, Caracas, Venezuela

Abstract

Pressure dependence of exchange interactions among small Mn clusters scattered throughout the network of sp^3 covalent bonds in a diluted magnetic semiconductor $Cd_{1-x}Mn_xSe$ has been studied by a cryobaric measurement of the exciton magnetophotoluminescence. The pressure is generated up to 2 GPa with a diamond anvil cell, being subjected at low temperatures to the static magnetic field up to 23 T generated with a hybrid magnet. The observed specific spin temperature T_0 of the clusters gives the effective internal exchange constant $J^*/k \equiv J_2/k + (10/3)J_3/k + 2J_4/k$ to be –2.0±0.4 K at 1 atm, where J_n denotes nth-neighbor exchange constant. The nearest-neighbor interaction constant is obtained to be J_1/k = -7.4±0.4 K at 1 atm from an analysis of the effect of the stepwise magnetization of Mn pairs. J^*, as well as J_1, increases rapidly with increasing pressure. The pressure coefficient $d\ln|J^*|/dP$ = 0.2-0.4 GPa^{-1} agrees with $d\ln|J_1|/dP$ = 0.25±0.05 GPa^{-1} within experimental errors. This result supports Larson's covalent spin interaction picture that the exchange interactions between the scattered, localized spins are determined by kinetic exchanges mediated by the extended p orbitals making the valence band of the host II-VI semiconductor.

Key Words. $Cd_{1-x}Mn_xSe$, diluted magnetic semiconductors, magnetophoto-luminescence, exchange interactions

I. INTRODUCTION

Hydrostatic pressure can compress a solid at a rate as high as an order of 1 % per 1 GPa in volume. Since a volume change over 1 % causes a large modification of the electron structure, various electronic properties of a material are influenced largely by a high pressure and the study of the effects provides a wealth of information on the nature of underlying physical processes. There have been a number of studies on the pressure dependence of the magnetism of magnetic materials. Among them the substances belonging to diluted magnetic semiconductors (DMSs) are unique in the sense that in the absence of a magnetic field they behave as ordinary semiconductors, while if a magnetic field is applied they exhibit unusual, strikng galvanomagnetic and magnetooptical properties. In DMSs transition metal elements are substituted for a fraction of 0.1 to 10 % of cations of host semiconductors. Their unique properties arise from strong interactions of electrons and/or holes of the host semiconductors with magnetic ions. The *s/p-d* hybridization is also an important ingredient. So far the pressure effects on those properties have been studied extensively.[1]

The magnetism of magnetic ions in a DMS depends on the electronic structure of the host semiconductor. For instance, *p*-type $Pb_{1-x-y}Sn_yMn_xTe$ of x=0.03 with a hole concentration of $5\text{-}10\times10^{20}$ cm^{-3} is a degenerate semiconductor but shows a ferromagnetic order due to Mn^{2+} spins below T_C of 2-4 K, which is determined by the hole concentration. Exploiting the property of this compound that the hole concentration can be tuned by pressure, Suski et al. [2] have shown the clear evidence that the ferromagnetic order arises from the Ruderman-Kittel-Kasuya-Yoshida (RKKY) interaction mediated by the degenerate holes. Pressure-induced switchover of the *d-d* interaction from an antiferromagnetic to ferromagnetic regime has been observed by Chudinov et al.[3] in the Shubnikov-de Haas experiment in *n*-type HgMnSe system. Since this material is a zero-gap DMS, under low pressures the Bloembergen-Roland and/or

kinetic superexchange mechanism dominates the *d*-*d* interactions.[4] According to Chudinov et al., pressure induces an energy gap, and as a result, like the case of $Pb_{1-x-y}Sn_yMn_xTe$, the RKKY mechanism tends to dominate the *d*-*d* interactions under high pressures.

In the present work we are concerned with the exchange mechanisms in the CdMnSe system, which is one of the wide-gap and nondegenerate II-VI DMSs. If Mn^{2+} ions are sufficiently dilute, they are scattered throughout the network of the semiconducting sp^3 covalent bonds. Turning our attention to the cation sublattice, we note that the majority of the Mn^{2+} ions are isolated and the rest form small clusters such as pairs, triads, quartets and so on.[5] For pairs in $Cd_{1-x}Mn_xSe$, it has recently been confirmed from cryobaric studies[6] of the exciton magnetophotoluminescence that the interaction between the two Mn^{2+} spins of a pair can be described well in terms of the kinetic superexchange theory based on the three-level model of Larson et al.[7], the model being comprised of the upper and lower Hubbard states of the *d* electrons and the valence band of anion *p* orbitals of the host semiconductor.

To date, however, the mechanism of interactions among the small clusters, including singles, has been controversial. Theoretically, by adapting the perturbation theory to their three-level model, Larson et al.[7] have argued that the kinetic (antiferromagnetic) exchanges mediated by the extended anion *p* states are responsible also for the second-neighbor and more distant interactions and that the exchange constant decreases rapidly with the radial distance *R* between two magnetic ions as

$$J = J_0 \exp(-4.89 r^2) \ , \ r = R/a , \qquad (1)$$

where *a* is $\sqrt{2}$ times the nearest-neighbor distance R_1 and J_0 is a constant giving $J = J_1$ for $r = r_1 \equiv 1/\sqrt{2}$, where J_1 is the nearest-neighbor exchange constant. In

addition to the work of Larson et al., several different relationships, that is, $J = J_1(r/r_1)^{-6.8}$, $J = J_1(r/r_1)^{-8.5}$, $J_2 = 2J_3 = 4J_4$ and $J_1 = J_2/(4\gamma) = J_3/(2\gamma) = J_4/\gamma = J_5/(4\gamma^2)$, have been proposed by Twardowski et al.[8], Rusin[9], Bruno and Lascaray[10] and Shen et al.[11], respectively, where the subscript n denotes nth-neighbor exchanges and γ is a numerical factor of the order of 0.04. The power laws are derived empirically[8] from the x dependence of the freezing temperature of a spin-glass state, or theoretically[9] within the framework of the three-level model. In contrast, the last two relationships are based on a different notion, named independent-exchange-path (IEP) model by Shen et al., that the strength of the interaction between a pair of localized spins of transition-metal ions is determined by the number of cation-anion bonds connecting the relevant ions. Bednarski et al.[12] have made a theoretical analysis of the magnetization profile in $Zn_{1-x}Mn_xTe$, $Zn_{1-x}Mn_xSe$ and $Cd_{1-x}Mn_xTe$ at low temperatures. Viewed from their result, the experimental magnetization data of the three Mn-based systems appear to favor the power law.

The purpose of the present study is to investigate which notion is valid in $Cd_{1-x}Mn_xSe$. Measurement of pressure dependence of the magnetization profile may give the decisive information on this problem, since pressure can change J_ns over a wide range without changing constituent elements. In particular, the information on the pressure dependence of the relative magnitudes of J_ns of $n \geq 2$ to J_1 would be cruicial. It is known that the magnetooptical spectroscopy of the band-gap exciton enables us to probe the magnetization of magnetic ions via the interaction of the exciton with the localized spins.[13] In fact, it has been established from the aforementioned cryobaric magnetophotoluminescence experiment by Kuroda and Matsuda[6] that J_1 in $Cd_{1-x}Mn_xSe$ of x =0.05 is enlarged prominently by pressure. In the present study, we examine the pressure dependence of J_ns of $n \geq 2$ in the CdMnSe system by using this technique.

There are several ways to evaluate J_ns of $n \geq 2$ in a DMS. One is to observe, as demonstrated by Vu et al.[14] with respect to $Zn_{1-x}Co_xTe$, the magnetization

steps due to second- and third-nearest-neighbor pairs. In Mn-based II-VI DMSs, however, the measurement of the J_2- and J_3-steps is difficult, because as discussed later J_2 and J_3 are so small that individual clusters behave as isolated ones under magnetic field. Instead, the interactions among clusters produce an internal magnetic field upon clusters themselves, and thus the spin temperature is altered by a specific temperature T_0, depending on x, from the lattice temperature.[15] In the present study we investigate the composition (x) and pressure dependencies of T_0. We discuss the result in comparison with the information on J_1, which is concurrently obtained from observation of the J_1-steps.

II. EXPERIMENT

Figure 1 shows the experimental setup for the cryobaric photoluminescence spectroscopy under strong magnetic field. An optical system[16] consisting of a diamond anvil cell (DAC) of clamp type and fiber optics is used to measure the near-gap photoluminescence radiation. The optical system is shown in Fig. 2. This system is designed to be suitable for combination with a hybrid magnet. The light beam from an Ar-ion laser, which is used as the light source to excite photoluminescence, is introduced into the optical chamber through a cable of glass fiber of core diameter 100 μm. The beam is focused on the sample in the diamond anvil cell using a lens (L1) and two prisms. To observe the near-gap photoluminescence the light radiated backward from the sample is collected with another lens (L2). The signal light is fed into a silica fiber of diameter 1.0 mm and then is guided to a multichannel spectrometer through a cable of bundled silica fibers. Here the laser beam is incident at an oblique angle on the diamond anvil, so that the flux of the beam reflected by the diamond and sample goes outside the aperture of the light collecting lens L2. Because of this optical geometry the fluorescence of fibers themselves is suppressed significantly. This is essential for observing a weak photoluminescence signal from the sample.

The diamonds used as anvils have a culet of 0.6 mm diameter, a girdle of 3.2 mm and a table of 2.0 mm. The gasket is a stainless-steel plate of thickness 0.2 mm. Pressure is generated in a 0.3 mm diam hole of the gasket. Condensed argon is employed as the pressure-transmitting medium. Argon is liquefied and loaded into DAC under atmospheric pressure using an apparatus that refrigerates the DAC together with the anvil-clamping jig with liquid nitrogen.[17] When the sample cell is filled with liquid argon, the cell is closed by clamping the diamond anvils. The DAC and jig are taken out of the apparatus when the whole system is warmed up to room temperature. Afterward, pressure is raised to an appropriate value.

Since the substances studied here undergo the structural phase transition to a dark rock-salt phase at 2-3 GPa, the pressure range is limited to 0-2 GPa in the present work. The optical system is immersed in liquid He at 4.2 K or in pumped superfluid He at 1.4 K. Static magnetic field up to 23 T generated with the hybrid magnet is applied parallel to the *c*-axis of the wurtzite crystal structure of the sample. The 514.5 nm line of an argon-ion laser is used as the light source to excite photoluminescence.

The value of pressure is deduced from the pressure-induced energy shift of the exciton photoluminescence band of the sample itself at zero magnetic field on the basis of the pressure versus energy gap relationship obtained from the absorption measurement at room temperature. In this absorption measurement a microscope-spectrometer system was used and the ruby fluorescence method was employed to calibrate pressure. An example of the pressure dependence of the fundamental absorption band is shown in Fig.3. The observed shift of the absorption edge is represented well as

$$E_G = E_{G0} + cP + dP^2 \quad , \qquad (2)$$

where P denotes pressure. The values of the coefficients c and d in the substances examined in this study are listed in Table I.

III. EXPERIMENTAL RESULTS

Figures 4, 5 and 6 show the photoluminescence energy of the A-exciton in $Cd_{1-x}Mn_xSe$ of x = 0.01, 0.05 and 0.10, respectively, as a function of magnetic field under various pressures at 1.4 K and 4.2 K. The observed state is the lower magnetic sublevel of the A-exciton which is originally of spin singlet. The large red shift is induced mainly by the exchange interactions of the exciton with Mn^{2+} ions magnetized by the magnetic field. If the distribution of the Mn^{2+} ions in the Cd sublattice is random, since the external magnetic field H is parallel to the c-axis, the observed photoluminescence energy is written in the mean field approximation as[17]

$$E_A = E_0 - \frac{1}{2} N_0(\alpha - \beta)x < S_z > -\frac{1}{2}(g_e - g_h)\mu_B H + \sigma H^2, \qquad (3)$$

where E_0 is the exciton energy at $H = 0$, $<S_z>$ is the absolute, mean value of S_z of Mn^{2+} spins, N_0 is the density of the Cd sublattice, α and β are the s-d and p-d exchange constants, respectively, g_e and g_h are g-parameters of a conduction electron and a hole, respectively, and σ is the coefficient of the diamagnetic shift of the A-exciton.

The Mn^{2+} clusters of which the ground states have nonzero total spins are magnetized continuously in the same manner as singles. Pairs, on the other hand, have a singlet ground state because of an antiferromagnetic coupling of the nearest-neighbor spins, so that they undergo a staircase-like magnetization. Let the probability that a Mn^{2+} ion can be regarded magnetically as a single be p_1*

and the probability that a Mn^{2+} ion forms a pair be p_2. Then, $<S_z>$ at temperature T can be expressed to a good approximation by[18-21]

$$< S_z >= p_1^* S B_S \left\{ \frac{2S\mu_B H}{k(T+T_0)} \right\} + \frac{p^2}{2} < S_z >_p \quad , \tag{4}$$

where $S = 5/2$, B_S is the normalized Brillouin function, μ_B is the Bohr magneton, T_0 is the specific spin temperature mentioned in Sec. I and $<S_z>_p$ is the absolute, mean value of S_z of a pair. We have

$$< S_z >_p = -\sum_{S_T=0}^{2S} \sum_{m=-S_T}^{S_T} m \exp\{-\frac{E_{p,m}}{k(T+T_p)}\} / \sum_{S_T=0}^{2S} \sum_{m=-S_T}^{S_T} \exp\{-\frac{E_{p,m}}{k(T+T_p)}\} \quad , \tag{5}$$

with

$$E_{p,m} = -J_1 \{S_T(S_T+1) - 2S(S+1)\} + 2\mu_B m(H - H_d), \tag{6}$$

where $E_{p,m}$ represents the Zeeman energy of a pair with a total spin S_T and a magnetic quantum number m; H_d is an internal field due to clusters surrounding the pair. The quantity T_p in Eq.(5) is a temperature parameter which is introduced to represent the broadening of the magnetization steps occurring at $H = H_j = -jJ_1/\mu_B + H_d$, $j = 1, 2, \cdots, 2S$.[22]

Theoretical curves of E_A are calculated with E_0, $N_0(\alpha\text{-}\beta)xp_1^*$, $N_0(\alpha\text{-}\beta)xp_2$, T_0, J_1 and T_p taken as adjustable parameters. The linear Zeeman energy $(g_e - g_h,)\mu_B H$, the diamagnetic shift σH^2 and the shift $-2\mu_B H_d$ are not negligible but are

very small compared with the total shift of E_A. Therefore g_e - g_h, σ and H_d are assumed to be independent of pressure. Referring to the literature their values are taken to be 1.7, 6.5×10^{-6} eV/T^2 and 0.7 T, respectively.

For x = 0.01, p_2 is so small compared to p_1* that we may neglect the energy part arising from pairs

$$E_s = -\frac{p_2}{4} N_0(\alpha - \beta) x < S_z >_p \quad . \tag{7}$$

The calculated curves of E_A-E_s are shown by dotted lines in Fig. 4. The contribution of E_s becomes significant for x = 0.05 and 0.10. The calculated curves of E_A-E_s and E_A for the compounds of x = 0.05 and 0.10 are shown by dotted and solid lines, respectively, in Figs. 5 and 6 along with the experimental data.

The spin-temperature parameter T_0 emerges from this analysis to be 0.7±0.3 K regardless of pressure in $Cd_{0.99}Mn_{0.01}Se$. The change in the value of T_0 due to pressure in this substance seems to be comparable to the experimental errors of ±0.3 K at most. As x increases, T_0 grows significantly. In the compounds of x = 0.05 and 0.10, T_0 amounts to 2.0±0.2 K and 2.6±0.4 K, respectively, at 1 atm. Accordingly they show an appreciable pressure dependence as shown in Fig. 7. The positive sign of T_0 means that the distant-neighbor interactions are antiferromagnetic. We see from Fig. 7 that the interactions are strengthened by pressure.

Figure 8 shows experimental and theoretical values of the contribution from pairs, -E_s, as a function of magnetic field in $Cd_{0.95}Mn_{0.05}Se$ under several pressures. The experimental values are obtained by subtracting the theoretical values of E_A-E_s from experimental values of E_A. Although the steps are broadened, the first and second steps can still be identified distinctly. At 1 atm,

they are located at 11.5 and 22.1 T, respectively. The positions of these steps yield J_1/k = -7.2±0.3 K at 1 atm. Similarly, for $Cd_{0.90}Mn_{0.10}Se$ we obtain J_1/k = -7.6±0.3 K at 1 atm. The average of these values of J_1/k is -7.4 K, which agrees within experimental errors with the value -7.6±0.2 K obtained by Forner et al.[21] As pressure increases, the steps are shifted towards higher magnetic fields because of the interplay of the enhancement of the *p-d* hybridization and the weakening of the onsite and intersite Coulomb energies U and V of Mn d electrons.[6] The values of $-J_1/k$ under various pressures are plotted in Fig. 9.

The exciton-Mn^{2+} exchange constant $N_0(\alpha-\beta)$ also changes with pressure, as reported elsewhere[6, 17]. In addition, the value of T_p is found to be in a range between 0.5 and 4.5 K and between 0.8 and 5.4 K for our samples of x = 0.05 and 0.10, respectively, showing a tendency to increase with pressure. However, the large part of the observed changes of T_p is likely to be produced by pressure-induced strains of crystals, because the changes are almost irreversible upon releasing pressure.

The experimental results presented above are summarized in Table II.

IV. DISCUSSION

1. Mean field approximation

Barilero et al.[15] have discussed the mechanism of T_0 in zincblende DMSs in the mean field approximation. They have argued that for a random distribution of Mn^{2+} ions T_0 is directly related to the internal exchange field produced by interactions among small clusters. In fact, as shown in Fig. 10, T_0 exhibits a systematic dependence on x. The internal field arises mainly from Mn-Mn interactions associated with the covalent bond pathways of the atomic sequence Mn-Se-Cd-Se-Mn: The difference in the spatial configuration of atoms in the crystal gives rise to the difference in the radial distance between the two terminating Mn sites.[10] Also shown in Fig. 10 are the experimental values of T_0

available for $Cd_{1-x}Mn_xSe$,[13] $Cd_{1-x}Mn_xS$,[18] $Cd_{1-x}Mn_xTe$,[18,23] $Zn_{1-x}Mn_xSe$,[23,24] and $Zn_{1-x}Mn_xTe$.[15] It is apparent from Fig.4.1 that Mn-based II-VI DMSs have similar properties of spin interactions.

The cation sites of a wurtzite crystal form a hcp sublattice. There are 6 second-nearest-neighbor sites at $R = a$, 2 third-nearest-neighbor sites at $R=\sqrt{4/3}a$, 18 fourth-nearest-neighbor sites at $R=\sqrt{3/2}a$ and 12 fifth-nearest-neighbor sites at $R=\sqrt{11/6}a$.[19] The third- and fourth-nearest-neighbor sites correspond to the third-nearest-neighbor sites at $R=\sqrt{3/2}a$ of the fcc sublattice of zincblende DMSs and the fifth-nearest-neighbor sites correspond to the fourth-nearest-neighbor sites at $R=\sqrt{2}a$ of the fcc sublattice. Approximating the third-nearest-neighbor exchange constant J_3' to be equal to the fourth-nearest-neighbor constant J_3 and reading the fifth-nearest-neighbor exchanges as the fourth-nearest-neighbor ones to make an argument parallel to Barilero et al., we have a relationship

$$kT_0 = -4xp_1^*S(S+1)J^* \quad , \tag{8}$$

with an effective internal exchange constant J^* of

$$J^* = J_2 + \frac{10}{3}J_3 + 2J_4 . \tag{9}$$

In a zincblende DMS, J^* is given by $J_2 + 4J_3 + 2J_4$. The contribution from pairs to this internal field is neglected in deriving Eq. (8), because the continuous magnetization of singles and single-like clusters, which is described by $B_S(H ; T+T_0)$, is sensitive to T_0 particularly in the low field region but pairs are in the

singlet ground state under magnetic field up to about 10 T, as we have seen in the preceding section.

Taking account of the internal fields due to clusters up to triads, p_1* can be written by the probabilities p_1, p_3, p_4 of singles, open triads and closed triads, respectively, as[15]

$$p_1^* = p_1 + \frac{p_3}{3} + \frac{p_4}{15}. \qquad (10)$$

If the contribution from clusters greater than triads is taken into account, the upper bound of p_1* is given by[25]

$$p_1^* = p_1 + \frac{p_3}{3} + \frac{p_4}{15} + \frac{1 - p_1 - p_2 - p_3 - p_4}{5}. \qquad (11)$$

If the distribution of Mn^{2+} ions in the hcp sublattice is random, the probabilities to find respective clusters are known to be[26]

$$\begin{aligned} p_1 &= (1-x)^{12}, \\ p_2 &= 12x(1-x)^{18}, \\ p_3 &= 18x^2(1-x)^{23}(7-5x), \\ p_4 &= 3x^2(1-x)^{21}\{7-6x+(1-x)^2\}. \end{aligned} \qquad (12)$$

For a fcc lattice, p_1, p_2 and p_3 are identical with those given by Eq. (12) but p_4 is replaced by $24x^2(1-x)^{22}$. Numerically, however, the difference in p_1* between hcp and fcc lattices is very small.

2. Analysis of the experimental data

To begin with let us look at the x dependence of $N_0(\alpha\text{-}\beta)xp_1$* and $N_0(\alpha\text{-}\beta)xp_2$. Figure 11 shows their experimental values at 1 atm as a function of x. The best-fit theoretical curves are also shown in Fig. 11 along with the experimental data. These theoretical curves are calculated from Eqs.(10), (11) and (12) with a common parameter of $N_0(\alpha\text{-}\beta)$ = 1.30 eV. The theoretical curves explain the experimental data of $N_0(\alpha\text{-}\beta)xp_1$* and $N_0(\alpha\text{-}\beta)xp_2$ well. The value of Eq.(10), which takes only the clusters smaller than quartets into account, disagrees to some extent with the experimental dada of $N_0(\alpha\text{-}\beta)xp_1$* for x = 0.1, but in view of the theoretical upper bound given by Eq. (11) the disagreement is rather reasonable. It turns out from these data that Mn^{2+} ions are distributed throughout the hcp sublattice at random, indeed.

The result shown in Fig. 11 assures also that the exchange interaction between an exciton and a Mn^{2+} ion is almost independent of x. In addition, as we have seen in Sec. III, our experimental values of J_1/k for x = 0.05 and 0.10 agree with each other within experimental errors. These findings suggest that Mn-Mn interactions are almost independent of x for the compounds of $x \leq 0.1$. Consequently, the observed x dependence of T_0 permits us to evaluate J* at a given pressure. In Fig. 10 the theoretical curves of T_0 calculated by putting Eqs.(10), (11) and J^*/k = -2.0 K into Eq.(8) are compared with experimental values at 1 atm. The mean field theory is found to explain the experimental data very well. Taking the experimental errors into account, the present data provide J^*/k to be –2.0±0.4 K at 1 atm.

We now proceed to the spatial variation of J. With the value of J_1/k = -7.4 K at 1 atm, the Gaussian form, $\exp(-4.89r^2)$, and power laws $r^{-8.5}$ and $r^{-6.8}$ predict T_0 = 0.89, 0.71 and 1.54 K, respectively, whereas the IEP model predicts T_0 = 4.3 K if Shen's γ of 0.044 is adapted. In Fig. 12 the photon energies E_A-E_s calculated by

putting these values of T_0 and $N_0(\alpha-\beta)xp_1^* =$ 37.0 meV into Eq. (3) are compared with our experimental data of E_A in $Cd_{0.95}Mn_{0.05}Se$ at 1.4 K and 1 atm. The calculated curves show striking differences from each other in a low-field region. This is because the initial slope scales with $T+T_0$ as $(T+T_0)^{-1}$. Twardowski's power law $r^{-6.8}$ matches the experimental data rather well but the other three laws mismatch the data significantly. If the exponent q of the power law r^{-q} is adjusted, our experimental data of J_1/k = -7.4 K and J^*/k = –2.0 K yield q = 6.1 with J_2/k = -0.89 K, J_3/k = -0.26 K and J_4/k = -0.14 K.

Although Larson's three-level model appears to underestimate J_n of $n \geq 2$, it puts forward the notion that the spatial variation of covalent spin interactions in II-VI DMSs can be expressed as $J = J_1 f(r)$ with a volume-independent function $f(r)$ of $f(1/\sqrt{2}) = 1$. This notion gives a physical basis to power laws.[9] The volume-independency is common to indirect interactions mediated by extended electronic states. In fact, a similar nature is also seen in the RKKY interaction. Apart from volume-dependent prefactors including the squared *s*-*d* exchange constant, the spatial dependence of the RKKY interaction obeys a function of the product $k_F R$ of the Fermi momentum k_F and R, and thus is invariable as long as the number of electrons forming the Fermi sphere is conserved. It is worth while to see how T_0 in $Cd_{1-x}Mn_xSe$ varies with pressure relatively to J_1. As seen in Fig. 7, the normalized pressure coefficient of T_0, that is, $d\ln T_0/dP$, which is equal to $d\ln|J^*|/dP$, is 0.24±0.1 GPa^{-1} in $Cd_{0.95}Mn_{0.05}Se$. This result agrees well with $d\ln|J_1|/dP$ = 0.25±0.05 GPa^{-1} indicated by the data of $Cd_{0.95}Mn_{0.05}Se$ and $Cd_{0.90}Mn_{0.10}Se$ in Fig. 9. Although $d\ln T_0/dP$ of 0.4±0.1 GPa^{-1} at x = 0.10 is a little larger than the value at x = 0.05, it is still comparable within experimental errors to $d\ln|J_1|/dP$.

The present result suggests that the power law r^{-q} holds even under high pressures, while retaining the exponent at $q \approx 6$. This finding supports Larson's covalent spin interaction picture that the exchange interactions between dilute

Mn^{2+} spins in the covalent bond network of a II-VI semiconductor are determined by kinetic exchanges mediated by the extended *p* orbitals making the valence band of the host semiconductor. Shen et al. have dealt with $Zn_{1-x}Mn_xTe$ of x = 0.938, in which Zn sites are mostly replaced by Mn, to deduce the IEP model. In such a dense magnetic alloy, the *d* electrons could have a significant itinerancy, and thus the dominant exchange mechanism could be different from that in usual DMSs.

V. SUMMARY

To study the nature of the distant-neighbor exchange interactions between localized spins in a wide-gap DMS, we have measured the Mn-composition and pressure dependencies of the exciton magnetophotoluminescence in $Cd_{1-x}Mn_xSe$ at low temperatures under high static magnetic field. Within the framework of a mean field approximation we have evaluated the effective internal exchange constant $J^* \equiv J_2+(10/3)J_3+2J_4$ from the observed x dependence of the specific spin temperature T_0 of small clusters of Mn^{2+} ions. We have also obtained the nearest-neighbor exchange constant J_1 from the observation of the staircase magnetization of Mn pairs under pressure. It has emerged that J^* increases with pressure with its normalized pressure coefficient nearly equal to that of J_1. This observation supports the covalent spin interaction picture that the spatial variation of J can be expressed as $J = J_1 f(r)$ with a volume-independent, short-range function $f(r)$ of the radial distance r. If the power law is employed for $f(r)$, the present experimental results give $J_n = J_1(r_n/r_1)^{-q}$ with $q \approx 6$.

ACKNOWLEDGMENTS

The experiments were performed at the High Field Laboratory for Superconducting Materials, Tohoku University. The authors (N.K. and Y.M.) are

grateful to K. Sai and Y. Ishikawa for operation of the high field magnets and helpful assistance throughout the whole course of the experiments**.**

* Present address, Institute for Solid State Physics, University of Tokyo, Tokyo 106, Japan.

†1 Present address, National Research Institute for Metals, Tsukuba 593, Japan.

[1] N. Kuroda, Semiconductors and Semimetals, edited by R. K. Willardson and R. Weber, Vol.54, High Pressure in Semiconductor Physics I, edited by T. Suski and W. Paul (Academic Press, 1998) Chap.6.

[2] T. Suski, J. Igalson, and T. Story, J. Mag. Mag. Mater., **66**, 325 (1987).

[3] S. M. Chudinov, D. Tu. Rodichev, G. Manici, and S. Sizza, Phys. Stat. Sol. (b), **175**, 213 (1993).

[4] N. B. Brandt, V. V. Moshchalkov, A. O. Orlov, L. Skrbek, I. M. Tsidil'kovski, and S. M. Chudinov, Sov. Phys. JETP 57, 614 (1983).

[5] S. Oseroff and P. H. Keesom, Semiconductors and Semimetals, edited by R. K. Willardson and A. C. Beer, Vol.25, Diluted Magnetic Semiconductors, edited by J. K. Furdyna and J. Kossut (Academic Press, 1988) Chap.3.

[6] N. Kuroda and Y. Matsuda, Phys. Rev. Lett. **77**, 1111 (1996).

[7] B. E. Larson, K. C. Hass, H. Ehrenreich, and A. E. Carlsson, Phys. Rev. **B37**, 4137 (1988).

[8] A. Twardowski, H. J. Swagten, W. J. M. de Jonge, and M. Demianiuk, Phys. Rev. **B36**, 7013 (1987).

[9] T. M. Rusin, Phys. Rev. **B53**, 12577 (1996).

[10] A. Bruno and J. P. Lascaray, Phys. Rev. **B38**, 9168 (1988).

[11]Q. Shen, H. Luo, and J. K. Furdyna, Phys. Rev. Lett. **75**, 2590 (1995).

[12]H. Bednarski, J. Cisowski and J. C. Portal, Phys. Rev. **B 55**, 15762 (1997).

[13] R. L. Aggarwal, S. N. Jasperson, J. Stankiewicz, Y. Shapira, S. Forner, B. Khazai and A. Wold, Phys. Rev. **B 28**, 6907 (1983).

[14]T. Q. Vu, V. Bindilatti, Y. Shapira, E. J. McNiff, Jr., C. C. Agosta, J. Papp, R. Kershaw, K. Dwight and A. Wold, Phys. Rev. **B 46**, 11617 (1992).

[15]G. Barilero, C. Rigaux, N. H. Hau, J. C. Picoche and W. Giriat, Solid State Commun. **62**, 345 (1987).

[16] Y. Matsuda, N. Kuroda, and Y. Nishina, Rev. Sci. Instrum. **63**, 5764 (1992)

[17] Y. Matsuda and N. Kuroda, Phys. Rev. **B53**, 4471 (1996).

[18] R. L. Aggarwal, S. N. Jasperson, P. Becla, and R. R. Galazka, Phys. Rev. **B 32**, 5132 (1985).

[19] B. E. Larson, K. C. Hass and R. L. Aggarwal, Phys. Rev. **B 33**, 1789 (1986).

[20]J. R. Anderson, Physica **B 164**, 67 (1990).

[21] S. Forner, Y. Shapira, D. Heiman, P. Becla, R. Kershaw, K. Dwight and A. Wold, Phys. Rev. **B 39**, 11793 (1989).

[22]Y. G. Rubo, M. F. Thorpe and N. Mousseau, Phys. Rev. **B 56**, 13094 (1997).

[23] Y. Shapira and N. F. Oliveira, Jr., Phys. Rev. **B 35**, 6888 (1987).

[24] W. Y. Yu, A. Twardowski, L. P. Fu, A. Petrou and B. T. Jonker, Phys. Rev. **B 51**, 9722 (1995).

[25] Y. Shapira, S. Forner, D. H. Ridgley, K. Dwight and A. Wold, Phys. Rev. **B 30**, 4021 (1984).

[26]R. E. Behringer, J. Chem. Phys. **29**, 573 (1958); M. M. Kreitman and

D. L. Barnett, ibid **43**, 364 (1965).

FIG. 1. Experimental setup for the cryobaric photoluminescence spectroscopy under strong magnetic field.

FIG. 2. Arrangement of a DAC and optics in the optical chamber.

FIG. 3. Fundamental absorption spectrum in $Cd_{0.95}Mn_{0.05}Se$ under various pressures at room temperature.

FIG. 4. Photoluminescence energy of exciton in $Cd_{0.99}Mn_{0.01}Se$ under magnetic field at 4.2 K at several pressures. The dittoed lines are the theoretical curves of E_A-E_s.

FIG. 5. Photoluminescence energy of exciton in $Cd_{0.95}Mn_{0.05}Se$ under magnetic field at 1.4 K at several pressures. The solid and dotted lines are the theoretical curves of E_A and E_A-E_s , respectively.

FIG. 6. Photoluminescence energy of exciton in $Cd_{0.90}Mn_{0.10}Se$ under magnetic field at 1.4 K and 4.2 K at several pressures. The solid and dotted lines are the theoretical curves of E_A and E_A-E_s , respectively.

FIG. 7. Pressure dependence of T_0 in $Cd_{0.95}Mn_{0.05}Se$ and $Cd_{0.90}Mn_{0.10}Se$.

FIG. 8. -E_s versus magnetic field at 1.4 K in $Cd_{0.95}Mn_{0.05}Se$ under several pressures. Solid lines are the theoretical curves. Vertical arrows show positions of H_1 and H_2.

FIG. 9. Pressure dependence of $-J_1/k$ in $Cd_{0.95}Mn_{0.05}Se$ and $Cd_{0.90}Mn_{0.10}Se$.

FIG. 10. The x dependence of T_0 in $Cd_{1-x}Mn_xSe$ at 1 atm. Reported experimental data for $Cd_{1-x}Mn_xSe$ (Ref.13), $Cd_{1-x}Mn_xS$ (Ref.23), $Cd_{1-x}Mn_xTe$ (Refs.18, 23), $Zn_{1-x}Mn_xSe$ (Refs.23, 24) and $Zn_{1-x}Mn_xTe$ (Ref.15) are also shown for comparison. The solid lines (a) and (b) are the theoretical curves calculated from Eq.(8) with p_1* given by Eqs.(10) and (11), respectively.

FIG. 11. The x dependence of of $N_0(\alpha-\beta)xp_1$* and $N_0(\alpha-\beta)xp_2$. The solid lines are the theoretical curves. The difference between lines (a) and (b) comes from the use of Eqs.(10) and (11), respectively, for p_1*.

FIG. 12. Comparison of theoretical curves with the experimental values of the exciton energy E_A in $Cd_{0.95}Mn_{0.05}Se$ under magnetic field at 1.4 K and 1 atm.

Table I. Values of the pressure coefficients *c* and *d* in $Cd_{1-x}Mn_xSe$.

x	*c* (meV/GPa)	*d* (meV/GPa^2)
0.01	59 ± 1	- 4.1 ± 0.6
0.05	55 ± 3	- 2.1 ± 1.3
0.10	54 ± 1	- 3.8 ± 0.4
0.25	44 ± 3	- 1.1 ± 1.3

Table II. Experimental values of J_1, T_0 and their pressure coefficient in $Cd_{1-x}Mn_xSe$.

x	J_1/k (K) at 1 atm	$d\ln\|J_1\|/dP$ (GPa^{-1})	T_0 (K) at 1 atm	$d\ln T_0/dP$ (GPa^{-1})
0.01	-	-	0.7±0.3	-
0.05	- 7.2±0.3	0.25±0.05	2.0±0.2	0.24±0.1
0.10	-7.6±0.2	0.25±0.05	2.6±0.4	0.4±0.1

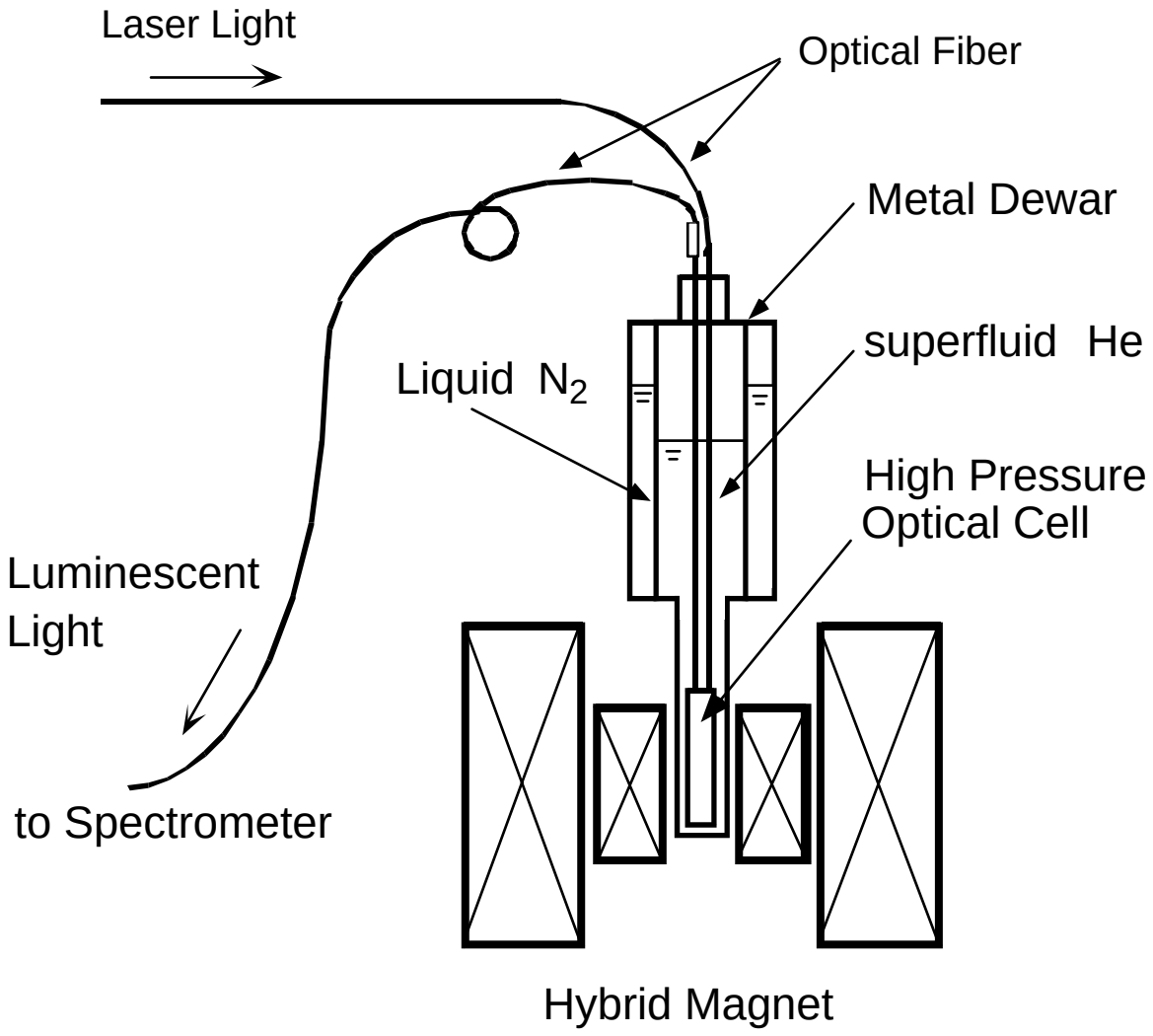
Laser Light
Optical Fiber
Metal Dewar
superfluid He
Liquid N_2
High Pressure
Optical Cell
Luminescent
Light
to Spectrometer
Hybrid Magnet

Fig. 1.

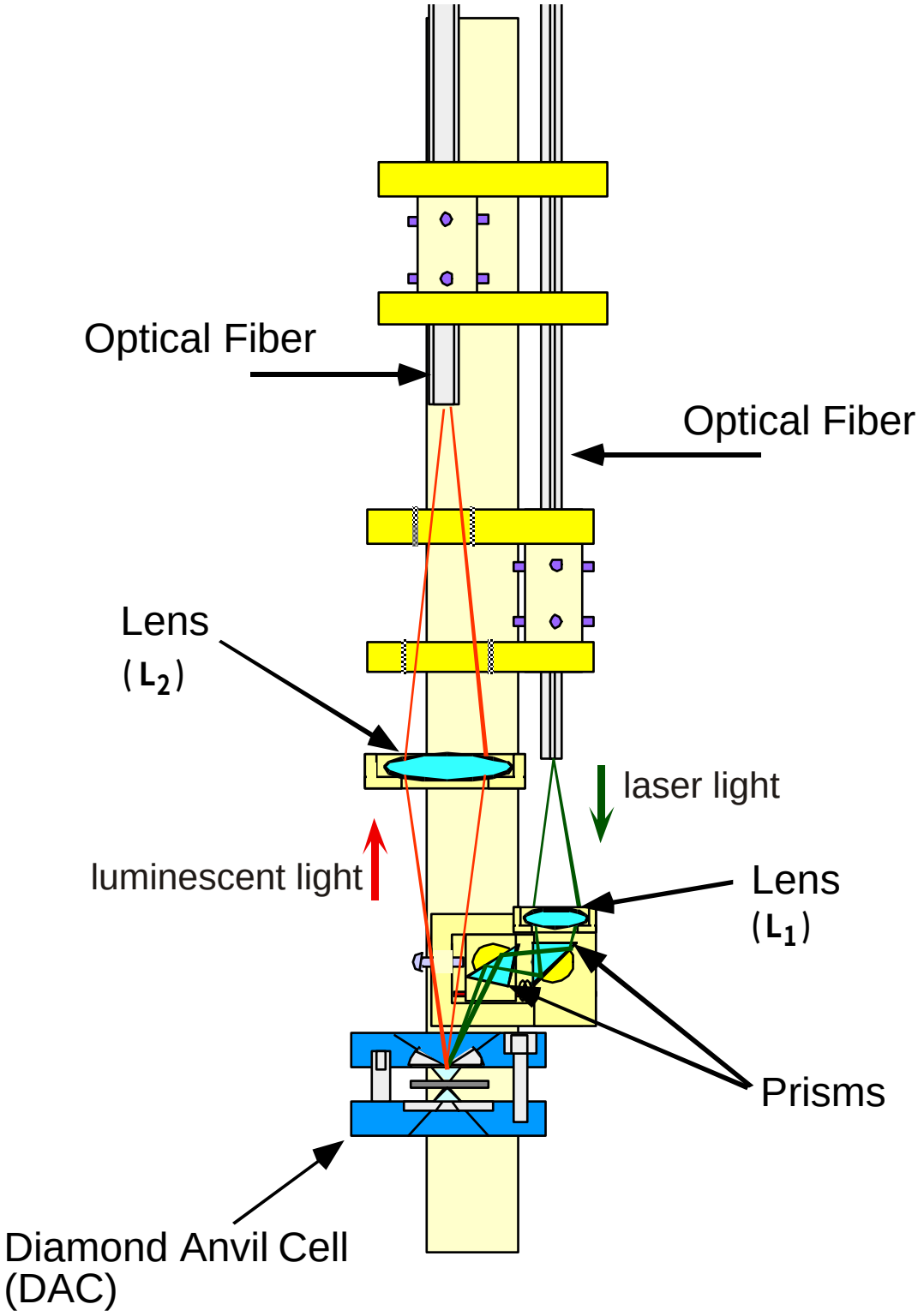
Optical Fiber
Optical Fiber
Lens
(L2)
laser light
luminescent light
Lens
(L1)
Prisms
Diamond Anvil Cell
(DAC)

Fig. 2.

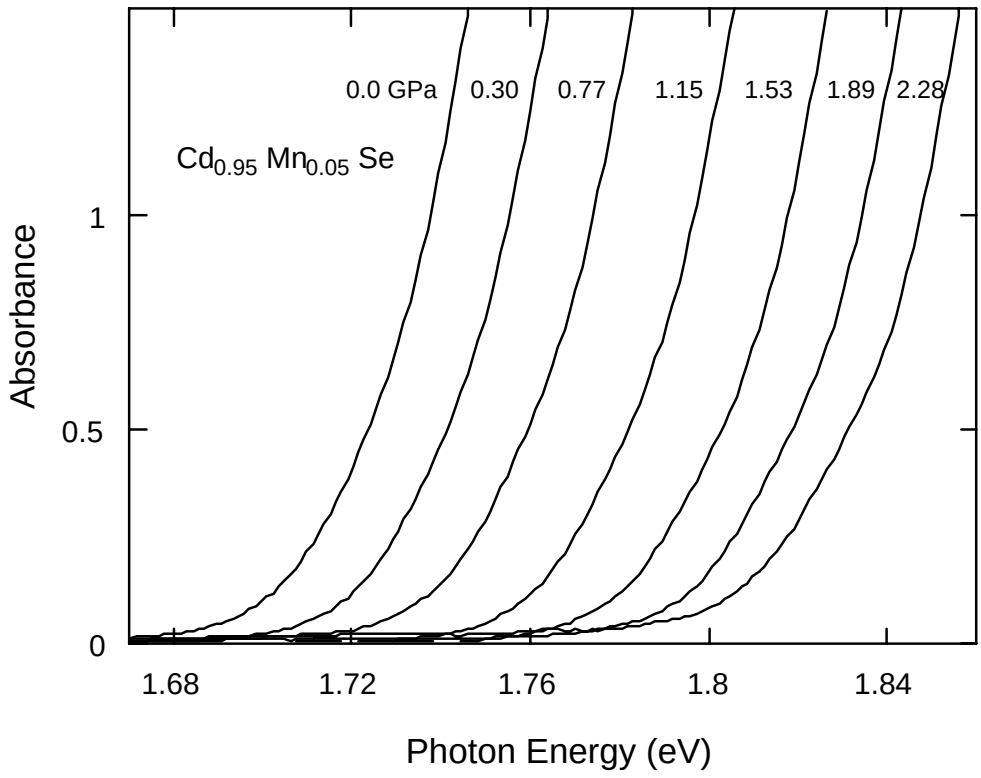
0.0 GPa
0.30
0.77
1.15
1.53
1.89
2.28
Cd0.95 Mn0.05 Se
Absorbance
1
0.5
0
1.68
1.72
1.76
1.8
1.84
Photon Energy (eV)

Fig. 3.

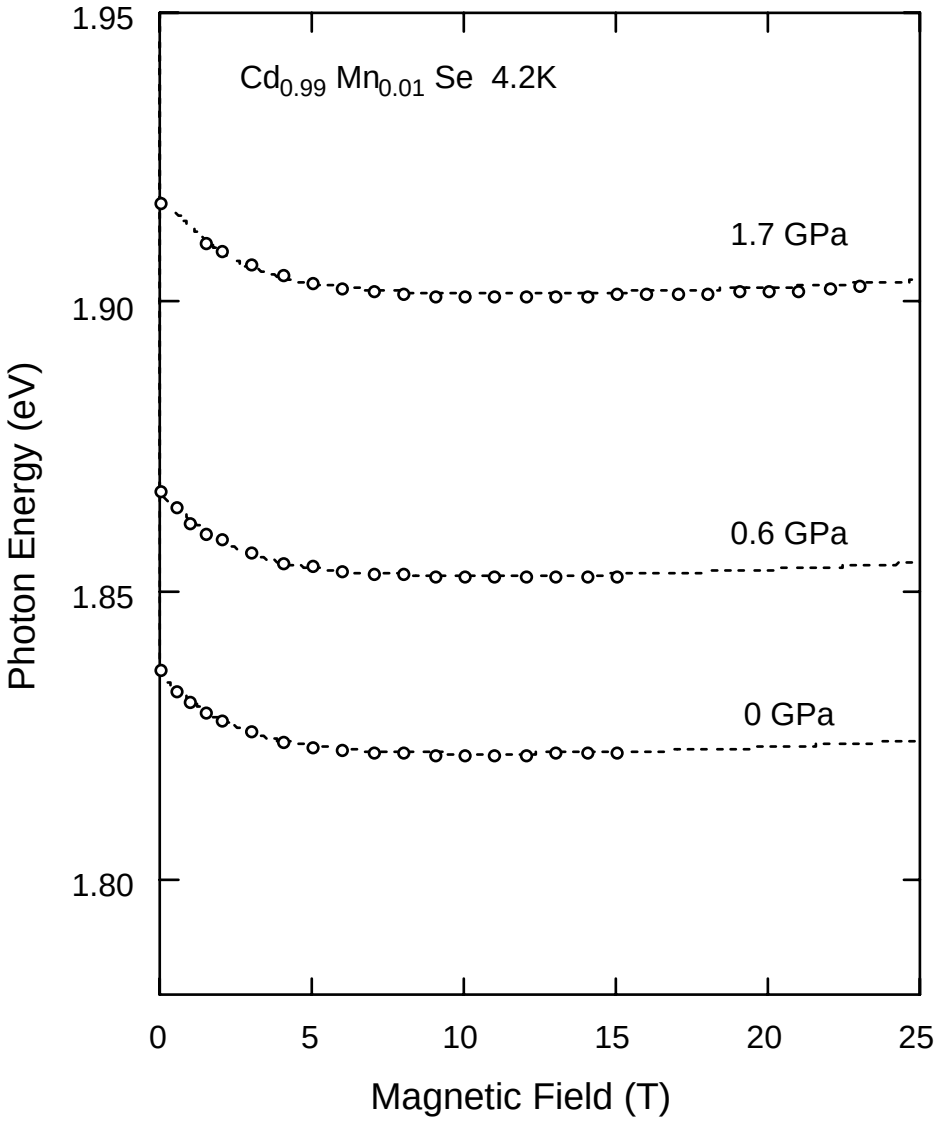
1.95
1.90
1.85
1.80
Photon Energy (eV)
Cd0.99 Mn0.01 Se 4.2K
1.7 GPa
0.6 GPa
0 GPa
0
5
10
15
20
25
Magnetic Field (T)

Fig. 4.

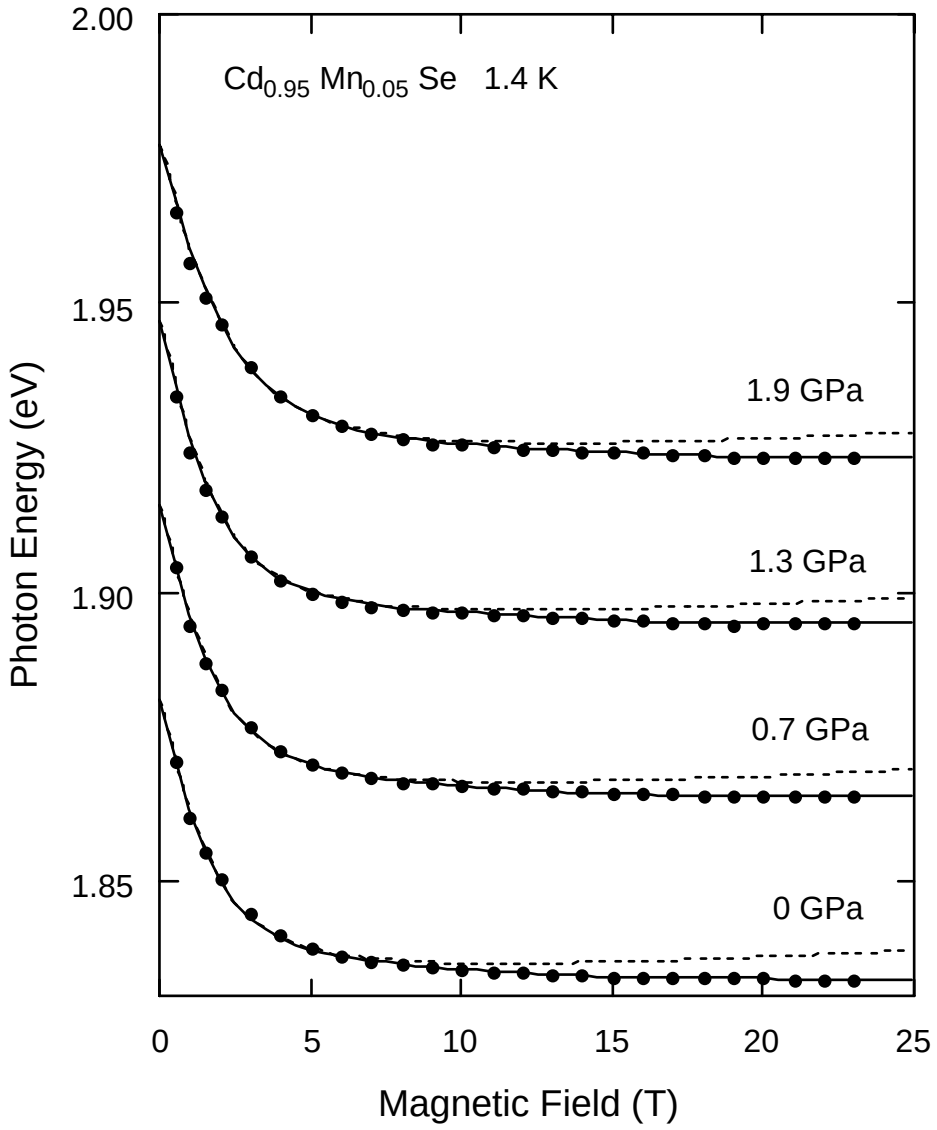
2.00
1.95
1.90
1.85
Photon Energy (eV)
Cd0.95 Mn0.05 Se 1.4 K
1.9 GPa
1.3 GPa
0.7 GPa
0 GPa
0
5
10
15
20
25
Magnetic Field (T)

Fig. 5.

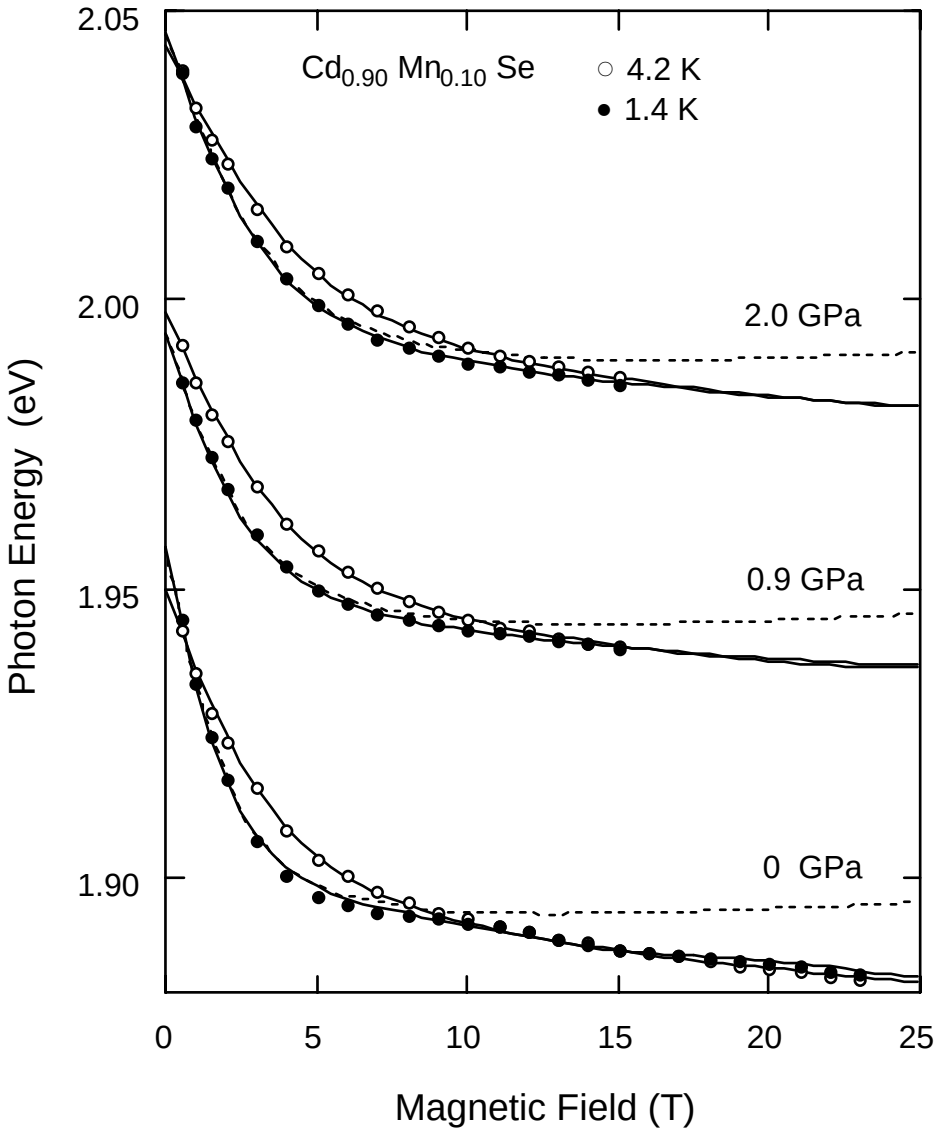
2.05
2.00
1.95
1.90
Photon Energy (eV)
Cd0.90 Mn0.10 Se
4.2 K
1.4 K
2.0 GPa
0.9 GPa
0 GPa
0
5
10
15
20
25
Magnetic Field (T)

Fig. 6.

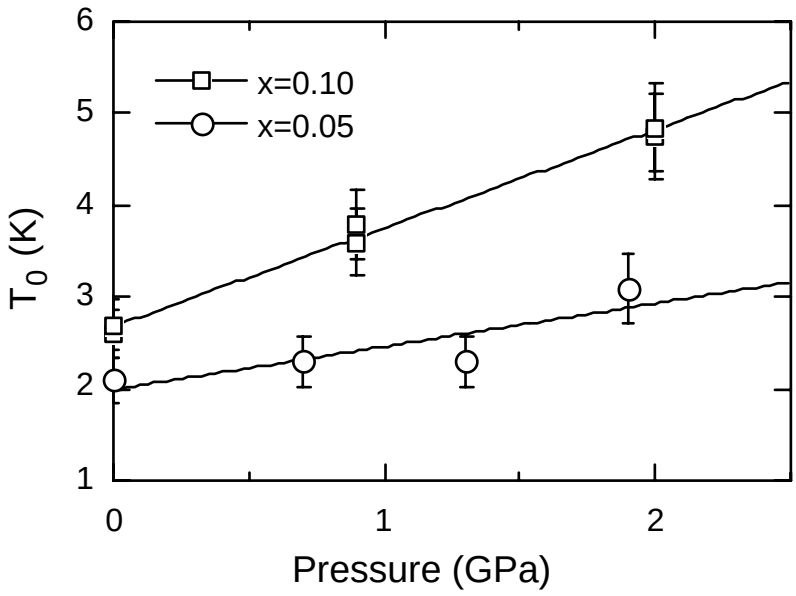

Fig. 7.

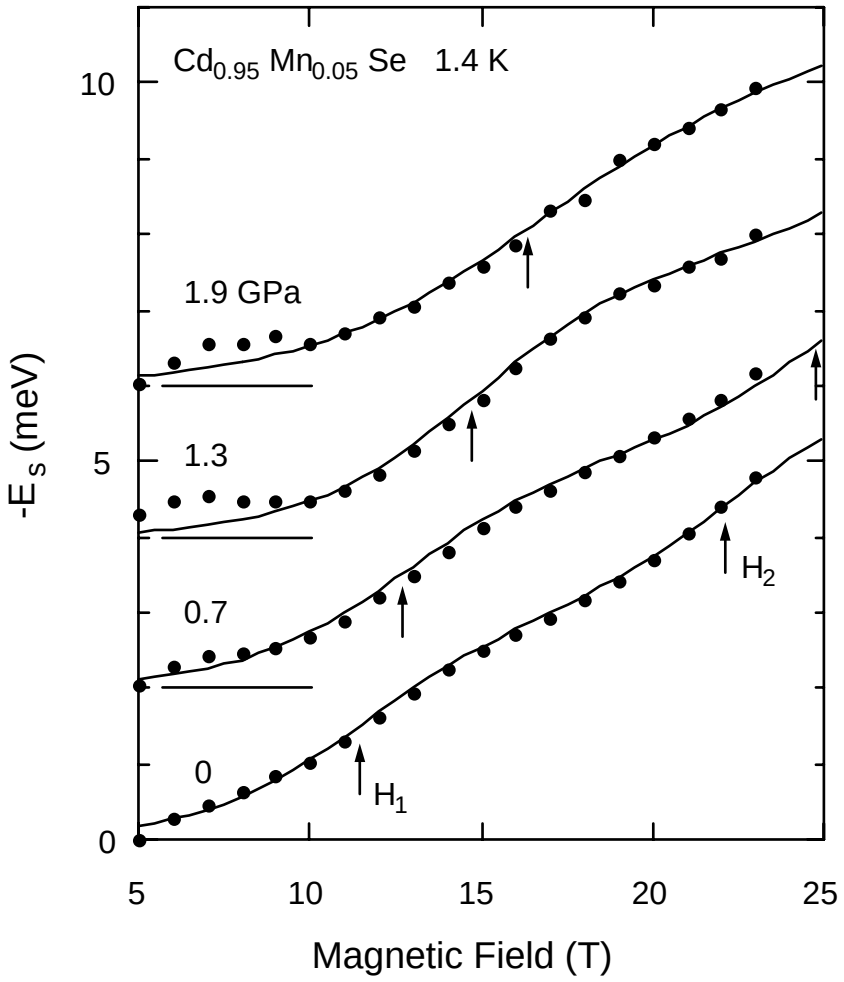
Cd0.95 Mn0.05 Se 1.4 K
1.9 GPa
1.3
0.7
0
H1
H2
-Es (meV)
Magnetic Field (T)
0
5
10
5
10
15
20
25

Fig. 8

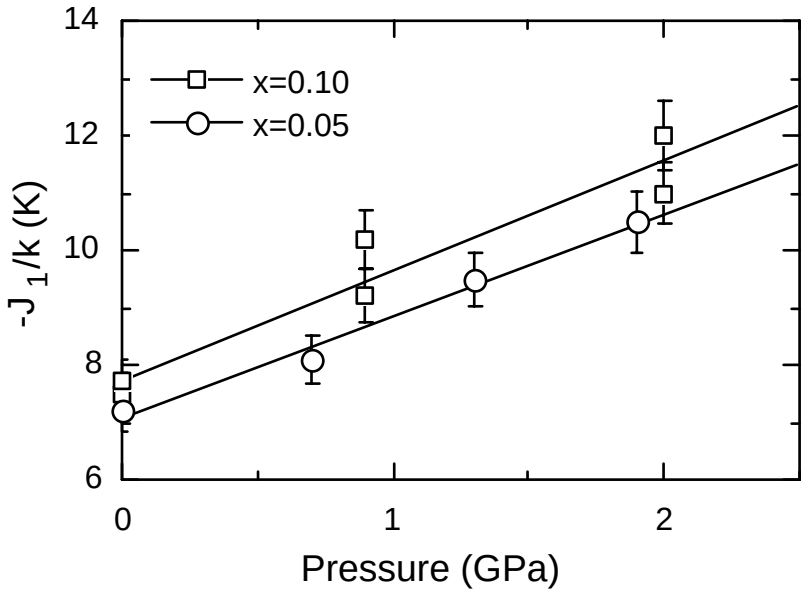

Fig. 9.

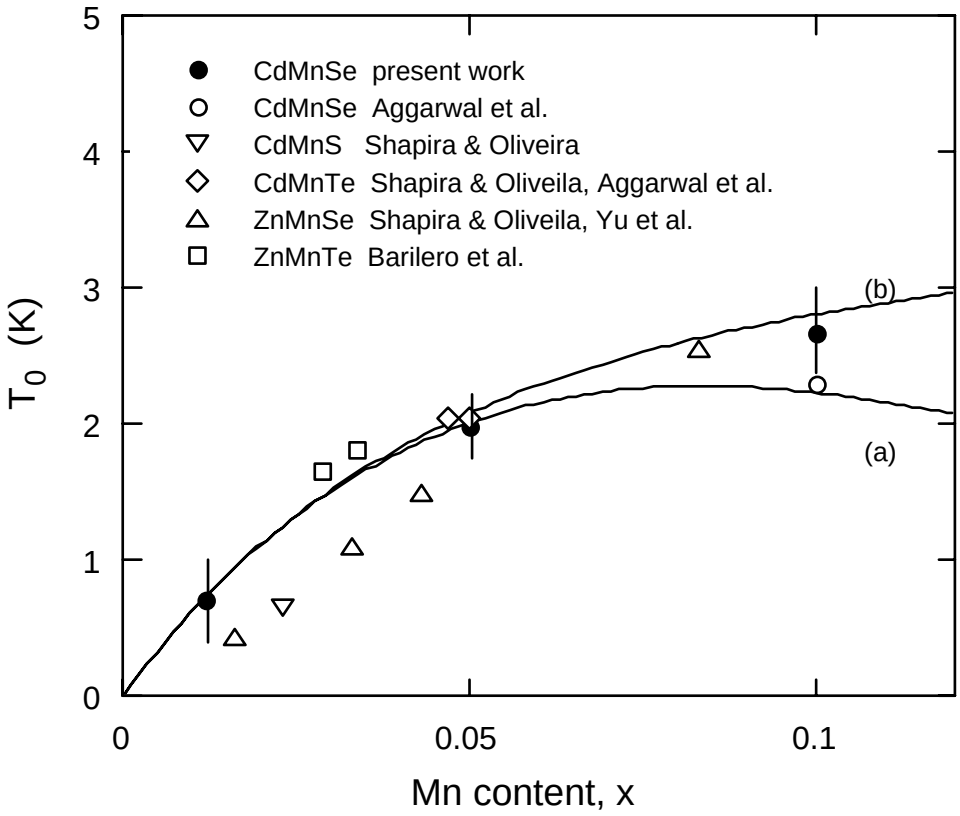
CdMnSe present work
CdMnSe Aggarwal et al.
CdMnS Shapira & Oliveira
CdMnTe Shapira & Oliveila, Aggarwal et al.
ZnMnSe Shapira & Oliveila, Yu et al.
ZnMnTe Barilero et al.
(b)
(a)
T_0 (K)
Mn content, x
0
1
2
3
4
5
0
0.05
0.1

Fig. 10.

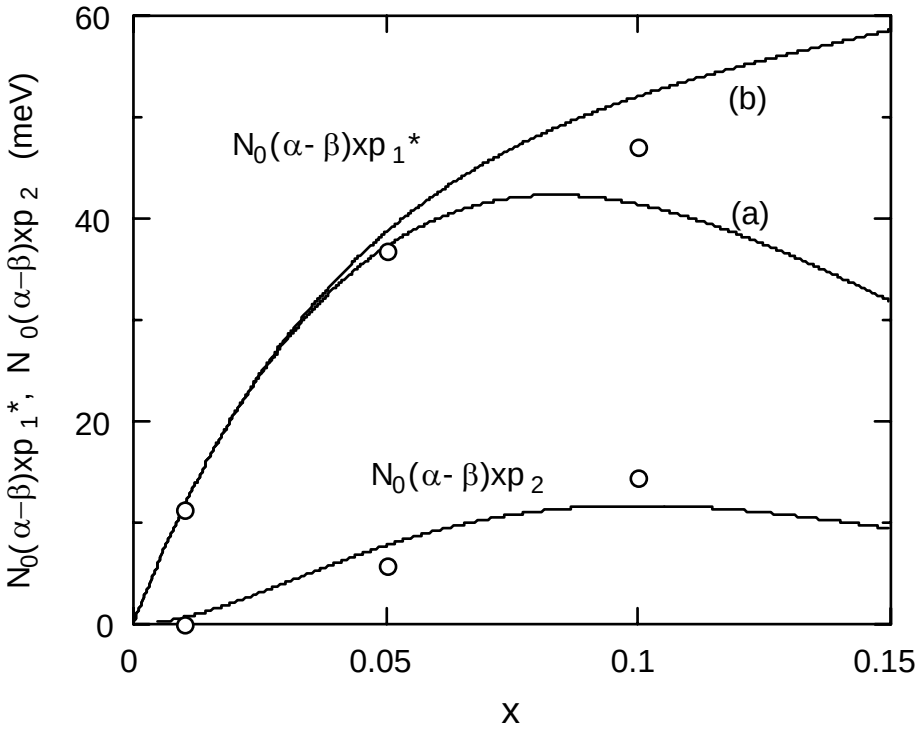
60
40
20
0
0
0.05
0.1
0.15
x
$N_0(\alpha-\beta)xp_1^*$, $N_0(\alpha-\beta)xp_2$ (meV)
$N_0(\alpha-\beta)xp_1^*$
$N_0(\alpha-\beta)xp_2$
(a)
(b)

Fig. 11.

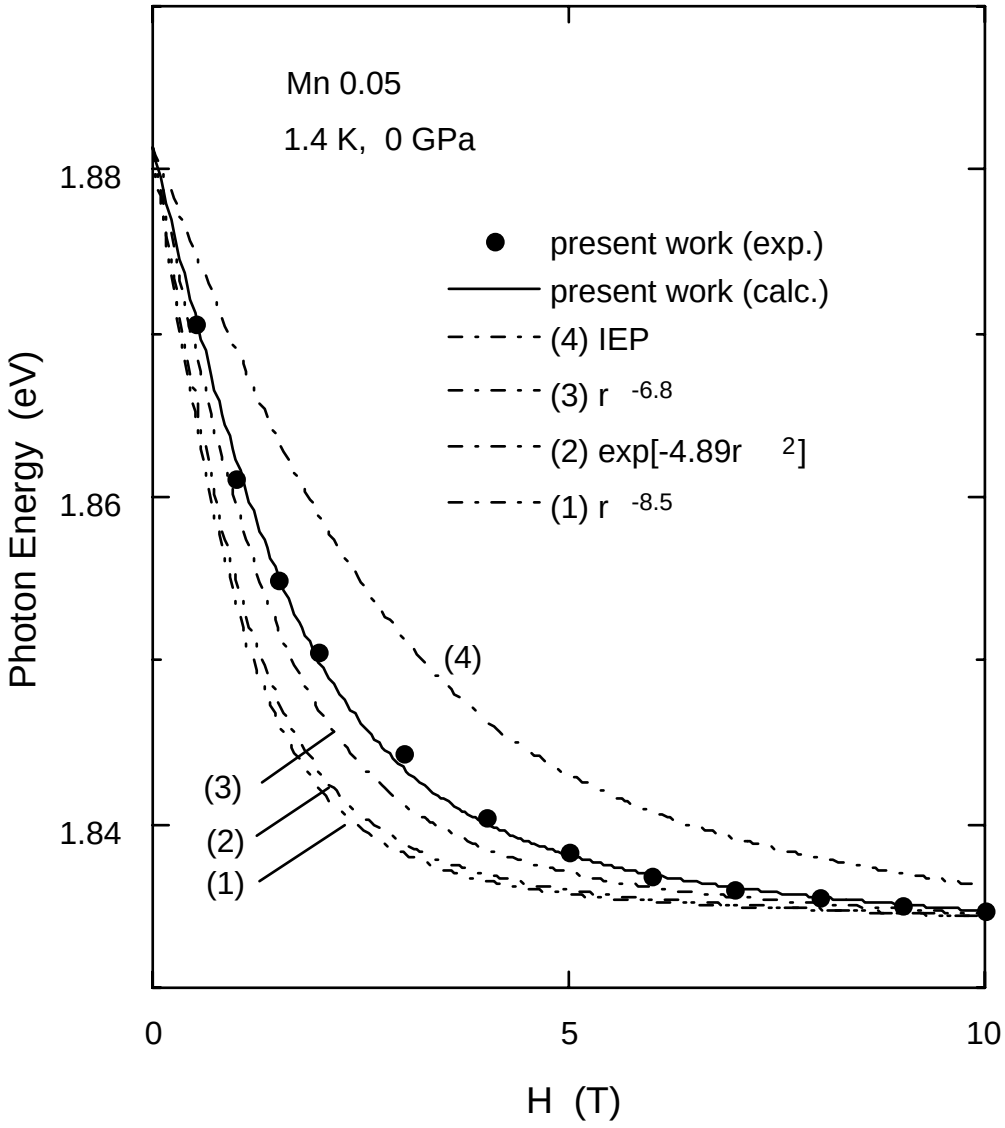
Mn 0.05
1.4 K, 0 GPa
present work (exp.)
present work (calc.)
(4) IEP
(3) r -6.8
(2) exp[-4.89r 2]
(1) r -8.5
Photon Energy (eV)
1.88
1.86
1.84
0
5
10
H (T)
(4)
(3)
(2)
(1)

Fig. 12.